Soil Moisture Drought in China, 1950–2006

AIHUI WANG

Nansen-Zhu International Research Centre, Institute of Atmospheric Physics, Beijing, China

DENNIS P. LETTENMAIER

Department of Civil and Environmental Engineering, University of Washington, Seattle, Washington

JUSTIN SHEFFIELD

Department of Civil and Environmental Engineering, Princeton University, Princeton, New Jersey

(Manuscript received 17 March 2010, in final form 19 November 2010)

ABSTRACT

Four physically based land surface hydrology models driven by a common observation-based 3-hourly meteorological dataset were used to simulate soil moisture over China for the period 1950–2006. Monthly values of total column soil moisture from the simulations were converted to percentiles and an ensemble method was applied to combine all model simulations into a multimodel ensemble from which agricultural drought severities and durations were estimated. A cluster analysis method and severity–area–duration (SAD) algorithm were applied to the soil moisture data to characterize drought spatial and temporal variability. For drought areas greater than 150 000 km^2 and durations longer than 3 months, a total of 76 droughts were identified during the 1950–2006 period. The duration of 50 of these droughts was less than 6 months. The five most prominent droughts, in terms of spatial extent and then duration, were identified. Of these, the drought of 1997–2003 was the most severe, accounting for the majority of the severity–area–duration envelope of events with areas smaller than 5 million km^2. The 1997–2003 drought was also pervasive in terms of both severity and spatial extent. It was also found that soil moisture in north central and northeastern China had significant downward trends, whereas most of Xinjiang, the Tibetan Plateau, and small areas of Yunnan province had significant upward trends. Regions with downward trends were larger than those with upward trends (37% versus 26% of the land area), implying that over the period of analysis, the country has become slightly drier in terms of soil moisture. Trends in drought severity, duration, and frequency suggest that soil moisture droughts have become more severe, prolonged, and frequent during the past 57 yr, especially for northeastern and central China, suggesting an increasing susceptibility to agricultural drought.

1. Introduction

Drought is recognized as one of the costliest of natural disasters. Severe drought can affect large regions and can persist for decades, as in the case of the 1930s ''Dust Bowl'' drought in the United States and the Sahel drought of the 1980s, among many others. While many regions in the world have suffered from droughts, China has experienced frequent severe droughts during the second half of twentieth century. Studies based on climate station data show that much of northern China has experienced droughts since the 1950s, with the most severe and prolonged droughts having occurred since 1990 (Qian et al. 2003; Wang et al. 2003; Zou et al. 2005; Xin et al. 2006; Zhai et al. 2010). For instance, Zou et al. (2005) calculated the Palmer Drought Severity Index (PDSI) for the period 1951–2003 over China and found that almost every year had more than 25% of the country under drought threat with the threshold of PDSI < -1.0. Zhai et al. (2010) also found large increases in dryness over northern China after 1990. The 2008/09 winter drought in northeastern China was one of the worst in the past 50 years, resulting in an estimated 16 billion Chinese yuan (2.3 billion U.S. dollars) in economic losses and subjecting more than 10

Corresponding author address: Aihui Wang, Nansen-Zhu International Research Centre, Institute of Atmospheric Physics, Chinese Academy of Sciences, P.O. Box 9804, Beijing 100029, China.
E-mail: wangaihui@mail.iap.ac.cn

DOI: 10.1175/2011JCLI3733.1

million people to water shortages. This drought is still developing (for more information, see http://news.xinhuanet.com/english/2009-02/04/content_10759053.htm).

Drought has especially impacted the agricultural areas of northern China. For instance, in 2000 drought damaged more than 40 million hectares of crops in northern China (Song et al. 2005). Wang et al. (2003), based on analysis of precipitation data, showed that the area in drought in northern China increased during 1950–2000, and that drought variations displayed multiple time scales and seasonal differences. The Yellow River has experienced prolonged periods of below normal flows in recent decades, resulting in complete drying of the river in some locations and periods. For example, a severe drought over northern China in 1997 resulted in 226 days of zero flow in the Yellow River from Henan to Shandong provinces. The total length of the river with zero flow was about 687 km (Liu and Zhang 2002; Xu 2004; Cong et al. 2009). Droughts have also frequently occurred in the Yangtze River basin during the past 50 years (e.g., Su et al. 2008; Zhai et al. 2010). The occurrence of severe droughts such as those mentioned here is usually related to a combination of precipitation and/or temperature anomalies, hydrological anomalies (e.g., low soil moisture or groundwater from previous seasons or years), terrestrial ecosystem conditions, and/or human activities (Woodhouse and Overpeck 1998; Understanding drought characteristics, including their duration, areal extent, and possible causes, is critical to understanding the nature of future droughts and eventually for forecasting of droughts, a science that is currently in its infancy (Svoboda et al. 2002; Sheffield et al. 2009).

Soil moisture modulates both the land surface water and energy cycles. Changes in soil moisture directly affect plant water availability, and in turn plant productivity and crop yields; hence, soil moisture deficits have critical implications for both agriculture and water supply. China lies within the Asian monsoon regime, and the summer and winter monsoons control precipitation variations in space and time over most of the country. The climate becomes wetter from north to south and from west to east. The northwestern regions are extremely arid, with some areas having no more than 100 mm of precipitation annually. Retention of soil moisture is especially important for agriculture in these dry areas. For this reason, soil moisture anomalies are often used as an index of agricultural drought.

Unfortunately, long-term measurements of soil moisture are only available at a few sites globally (e.g., Robock et al. 2000), and the density of stations is far too sparse and the time span of observations is too short to support drought studies. Remote sensing provides an alternative source of soil moisture measurements. However, satellite sensors provide estimates of the water content only of the upper few centimeters of soil (depending on their wavelength). While the recent (November 2009) launch of the European Soil Moisture and Ocean Salinity (SMOS) mission and planned launch of the U.S. Soil Moisture Active Passive (SMAP) mission will provide observations targeted directly at soil moisture, the current generation of satellite sensors has wavelengths too short to provide a viable source of soil moisture information over larger areas, and short record lengths will continue to be an issue even in the SMOS and SMAP era.

As an alternative to in situ and remotely sensed soil moisture, numerical model simulations have been used as a source of soil moisture information for drought studies (Sheffield et al. 2004, 2009; Sheffield and Wood 2007; Andreadis et al. 2005; Wang et al. 2009). Land surface models (LSMs) coupled with atmospheric models (e.g., Schubert et al. 2008) or driven offline by observed meteorological forcings can reproduce land surface water and energy variations. For example, Sheffield et al. (2004) derived a hydrologically based drought index based on simulated soil moisture and showed that it was able to reproduce drought occurrence and severity characteristics over the continental United States. Andreadis et al. (2005) developed an approach that they termed severity–area–duration (SAD) analysis, an adaptation of the depth–area–duration approaches widely used in design storm analysis, to characterize drought over the continental United States for the period 1916–2003. They used total column soil moisture simulations from the variable infiltration capacity (VIC) model. Wang et al. (2009) showed that plausible results were produced when the same methods were applied to other LSMs. Sheffield et al. (2009) extended the SAD approach to investigate global drought during 1950–2000 using total column soil moisture derived using the VIC model.

The accuracy with which hydrologic variables, including soil moisture, can be reproduced using offline applications of LSMs is strongly dependent on the quality of the meteorological forcing data and the physical parameterizations in the LSM. Given the same meteorological forcings and land surface properties (e.g., soils, topography, vegetation), simulations from different models can show disparities. Comparison of model-simulated soil moisture with in situ measurements generally shows that models poorly simulate actual soil moisture, but the models are able to reproduce anomalies and seasonal variability (Entin et al. 2000; Guo and Dirmeyer 2006). Because the representations of soil hydrology differ from model to model, the variability of soil moisture is highly model dependent. On the other hand, when appropriately normalized to have the same range and variability, model-derived soil moisture is generally much more consistent across models. Wang et al. (2009) investigated the performance of six LSMs with

respect to their ability to reproduce agricultural (soil moisture) drought characteristics over the continental United States for a simulation period of almost 100 years. Their approach to standardizing the soil moisture output was to express each model's monthly soil moisture as a percentile relative to that month's historical simulations; hence, all values were reformulated as uniformly distributed (between 0 and 1) variables. The results showed a general consistency in the representation of major droughts and thus the value of using the multimodel ensemble as a means of combining the estimates from the individual models.

In this paper, we utilize the multimodel approach developed in Wang et al. (2009) to reconstruct soil moisture in China, with particular emphasis on droughts. The paper is organized as follows: section 2 describes the models and data used in this study; the data analysis and statistical methods are described in section 3; section 4 investigates drought spatial and temporal variability as estimated from the multimodel ensemble derived soil moisture; and section 5 provides a summary and conclusions.

2. Models and data description

The soil moisture variables used in this paper come from four land surface models: 1) VIC (Liang et al. 1994); 2) the Community Land Model, version 3.5 (CLM3.5; Oleson et al. 2007, 2008); 3) Noah version 2.7 (Mitchell et al. 2001) with an updated snow albedo scheme (Livneh et al. 2010); and 4) a hybrid of CLM3.5 with the VIC soil hydrology scheme (CLM-VIC; Wang et al. 2008). The details of the structure and model physical processes are described in the references given above. All models were forced at the land surface with precipitation, surface air temperature, surface wind, vapor pressure deficit, and downward solar and longwave radiation. The models close the surface water budget by producing as prognostic variables runoff and evapotranspiration, with snow water equivalent and soil moisture as state variables. They close the surface energy budget concurrently by solving for the effective surface temperature (and depth profile of temperature) as a state variable, with reflected shortwave and emitted longwave radiation as prognostic variables. The performance of the four models have been extensively studied at both single stations and over larger areas or watersheds (globally in some cases; e.g., Chen et al. 1997; Nijssen et al. 2001; Maurer et al. 2002; Ek et al. 2003; Dickinson et al. 2006; Oleson et al. 2007; Wang et al. 2008, 2009).

Soil column representations and the parameterizations used for soil water movement differ considerably among the models. The total soil depth in CLM3.5 is fixed at 3.43 m and is divided into 10 layers with increasing soil layer thickness from upper to lower layers. In VIC and CLM-VIC, the layer depths differ from grid cell to grid cell. The total soil column in these two models can be as deep as 3 m [values extracted from the VIC global parameter set constructed by Nijssen et al. (2001)]. In the Noah model, the deepest total soil column depth is fixed at 2 m, and the layer depths are fixed at 10 cm, 30 cm, 60 cm, and 1 m, respectively. The different soil column depths result in disparities in the soil water holding capacity among models and lead to large differences in the simulated mean soil moisture amount. All of the models require that certain soil and vegetation parameters that describe the land system (e.g., soil water holding capacities, hydraulic conductivities, thermal conductivities and capacities, vegetation types, etc.) be specified, and these parameters differ from model to model. We have used herein ''off the shelf'' model parameters that have been estimated or calibrated for the model domain in previous studies. We did so to avoid influencing uncertainties in each model's representation of drought by introducing potentially inappropriate parameter values. While our general approach is similar to that used in Wang et al. (2009), the specific data sources vary somewhat. For CLM3.5, soil data were derived from the International Geosphere–Biosphere Programme (IGBP) soil dataset (Bonan et al. 2002), with vegetation parameters derived from Moderate Resolution Imaging Spectroradiometer (MODIS; Lawrence and Chase 2007) imagery. For the VIC model, soils data were derived from the Food and Agriculture Association (FAO)–United Nations Educational, Scientific and Cultural Organization (UNESCO) digital soil map of the world with the World Inventory of Soil Emission Potentials (WISE), using methods described in Nijssen et al. (2001). For the Noah model, parameters were taken from multiple sources: soil data, green vegetation fraction, and snow-free albedo were retrieved from the global dataset of Matthews (1984, 1985) and vegetation type was taken from the University of Maryland 1-km vegetation class dataset (Hansen et al. 2000). Because CLM-VIC is CLM3.5 merged with the VIC soil hydrology scheme, the CLM-VIC model used the same soil data as the VIC model. The vegetation scheme in CLM-VIC is identical to that in CLM3.5 and so the same vegetation data were used in both models.

All models were driven by a common meteorological dataset, which is a hybrid of data from the National Centers for Environmental Prediction (NCEP)–National Center for Atmospheric Research (NCAR) reanalysis (Kalnay et al. 1996) and a suite of global observation-based products. Details of the dataset are described in Sheffield et al. (2006). The dataset has been used to evaluate the global terrestrial water budget (Sheffield and Wood 2007) and also to drive the VIC model for exploration of global drought characteristics (Sheffield et al.

2009). The dataset used in this paper was extended to 2006 using the same approach as in Sheffield et al. (2006) to produce the original dataset, which spanned the period 1948–2000. The extension was based on updated versions (to 2006) of the underlying observations for precipitation, temperature (CRU 3.0; Mitchell and Jones 2005), and radiation (SRB 3.0; Gupta et al. 2006). The horizontal resolution of the original Sheffield et al. (2006) dataset was 1° × 1°, with a temporal resolution of 3 h. In this study, we first interpolated the global data to 0.5° spatial resolution using a bilinear interpolation method, and we then extracted the forcing data within the study domain. At 0.5° spatial resolution, the Chinese land area consisted of 3880 grid cells. We recognize that the raw (station) data that underlie the gridded dataset are somewhat sparser than the 0.5° resolution we used. On the other hand, the topographic, soil, and vegetation data have considerably finer spatial resolution. Our choice to use 0.5° as our model resolution represents a compromise between these two considerations. Sheffield et al. (2006) demonstrated that when the data were interpolated from 2° to 1° using the same bilinear interpolation method that we applied, some biases appeared in the foothill regions of major mountain ranges. We therefore compared the 0.5° elevation data interpolated from 1° to 0.5° dataset and found no prominent differences except in the vicinity of the southern foot of the Himalayas, which constitutes a small part of the entire domain (not shown). On this basis, we decided not to adjust the interpolated data. It is also worth noting that for drought studies such as this one, modest spatial variations in precipitation are somewhat less important than for other applications, since droughts tend to cover relatively large areas and to reflect accumulated precipitation deficits rather than short-term variations.

Our simulations were performed using a 1-h time step and 0.5° spatial resolution (the hourly data were linearly interpolated from the original 3-h time step data). To eliminate model initialization effects, all models were first run for 10 yr by cycling the forcing data for 1948 initialized with a specified intermediate soil wetness. The models were then run from 1948 to 2006, initialized with the final year of the spinup run. The annual precipitation for 1948 over much of China is slightly higher than the mean climatology (not shown), so the initialization described above might give a slightly wet initial condition. However, our analysis started with 1950, which should help to dissipate any modest initialization influences.

3. Methodology

Following Andreadis et al. (2005) and Sheffield et al. (2009), we defined drought as occurring when soil moisture values (percentiles) fall below a threshold value continuously in time over a contiguous area. We then used monthly soil moisture percentiles from the four LSMs to form a multimodel ensemble dataset, as described below. Drought events were identified from the multimodel dataset using the same cluster analysis approach as in Andreadis et al. (2005). Their method searches for temporally continuous and spatially contiguous areas in drought. SAD analysis is then applied to the space–time characteristics of these events. We also analyzed droughts on a grid cell by grid cell basis in terms of long-term trends in drought characteristics, such as duration and severity of soil moisture deficits.

a. Multimodel ensemble scheme

As noted above, previous work (e.g., Koster et al. 2009; Wang et al. 2009) indicates the intermodel variations are considerably reduced when the simulated soil moisture values are appropriately normalized. Our approach to doing so consisted of three steps. First, simulated (total column) soil moisture was converted to percentiles using the time series values of total column soil moisture for each model for each month in the period 1950–2006. Second, the median values of the monthly percentiles derived from the four models were computed at each grid cell to form a unified percentile time series for that grid cell. We found that one of the models (CLM 3.5) had some anomalous drift in very dry areas (caused by the model's very small interannual range in total column soil moisture in very dry areas). For this reason, we used the multimodel median, rather than the mean, notwithstanding that an exploratory analysis showed that this choice makes little difference to the character of the inferred multimodel drought. Finally, at each grid cell and for each month, the median (over models) percentile time series was again converted to a new percentile according to the empirical probability distribution of the median percentiles. This third step had only a minor effect on midrange soil moisture values; however, it corrects the tails of the averaged percentile distribution, which otherwise would deemphasize extremes. Stated otherwise, this step assures that the multimodel variable has a uniform distribution—without this step, extreme low or high values do not occur as often as in the percentile series from the individual models. Finally, the ensemble soil moisture percentiles were used to identify droughts as follows. A drought was defined as any percentile below 20%, as in previous drought identification work (Andreadis et al. 2005; Sheffield et al. 2009; Wang et al. 2009). It is also a threshold used in the U.S. Drought Monitor (see http://drought.unl.edu/dm/archive/99/classify.htm). We note that notwithstanding this step, the multimodel ensemble is expected to be smoother in both space and time than the space–time variations of the individual models. We view

this as a desirable outcome of the multimodel ensemble processing.

b. Clustering algorithm and severity–area–duration analysis for drought identification

The clustering algorithm developed by Andreadis et al. (2005) was used to identify drought spatial and temporal variations. The algorithm combines both spatially and temporally contiguous regions with soil moisture percentiles below the specified (20th percentile) value. For a specified minimum area, droughts are allowed to break up to form subdroughts or merge to form new larger droughts with time. The minimum area threshold was taken as 25 000 km^2 in previous work over the continental U.S. domain (Andreadis et al. 2005; Wang et al. 2009) and 500 000 km^2 for a study of global land areas by Sheffield et al. (2009). Sheffield et al. (2009) found that drought clusters with smaller (e.g., 25 000 km^2) thresholds could shrink to a few grid cells and persist many years through tenuous spatial connectivity. To avoid this situation, we set a minimum threshold of 150 000 km^2. In section 4d, we examine the sensitivity of the results to this threshold.

We used the severity–area–duration analysis approach of Andreadis et al. (2005) as a supplementary tool to characterize drought events. SAD is based on the widely used depth–area–duration (DAD) technique (Grebner and Roesch 1997) used for design storm analysis. We applied the method as in Andreadis et al. (2005); the only difference is that our percentile variants were the percentiles of the multimodel medians computed as described above, whereas in Andreadis et al. the percentiles were from a single model. In brief, the severity (S) in SAD is defined as $S = (1 - \Sigma P/t)$, where in our case P is the monthly ensemble median soil moisture percentile and ΣP is their sum over a duration of t months. The severity was calculated at each grid cell within the drought event as identified by the cluster analysis, implemented as in Andreadis et al. (2005), and then averaged over the drought area. The averaged drought severity for an event was calculated for time intervals within the lifetime of the event (3, 6, 12, 24, and 48 months, where the specific period within the event lifetime was picked to maximize the severity) and for subareas within the spatial domain of the event (starting from 150 000 km^2, which is about 60 grid cells—also selected so as to maximize the severity for the given subarea). Within each drought cluster, SAD treats the grid cell with the maximum severity to be the center of the drought and then adjoining grid cells with the next largest severity are added to form an intermediate drought cluster. In our application, this procedure continued in area increments of 20 grid cells (or 50 000 km^2) until the maximum spatial extent of the drought event was reached for a specified average severity over the specified drought length. The SAD algorithm provides a way to estimate an absolute drought magnitude without being constrained to an individual basin or area (Sheffield et al. 2009). As in Andreadis et al. (2005), following identification of all drought events during the study period, the maximum severities of all events at each area increment were selected to form SAD envelope curves, which represent the most severe events during the period of record for each area and duration.

c. Trend analysis and estimation of field significance

Nonparametric trend tests have been widely used in hydrology. The Mann–Kendall (MK) test (Mann 1945), for instance, is extensively used for testing of monotonic (e.g., linear) trends. In its classical form, the MK test requires an assumption of independence, which is often approximately met for annual (but not seasonal) data. On the other hand, soil moisture usually has substantial memory at monthly and finer time intervals; that is, the monthly soil moisture is usually autocorrelated. Hamed and Rao (1998) proposed a modified MK test for autocorrelated data. Hirsch et al. (1982) proposed an alternative formulation of the MK test for use with seasonal data. Their test has been applied both to observed climate and hydrological variables (e.g., Lettenmaier et al. 1994) and to model-derived hydrological variables (e.g., Andreadis and Lettenmaier 2006). We applied the Hirsch et al. (1982) method to the monthly time series of soil moisture, drought severity, duration, and frequency as in Andreadis and Lettenmaier (2006).

Spatial correlation among climate variables is another complication that reduces the degrees of freedom when assessing regional trends. Livezey and Chen (1983) proposed a method wherein both a local significance (significance level of a test if applied at a single location individually) and a field significance (which pertains to the number of locations at which the null hypothesis has to be rejected at the local significance level). The field significance level is calculated based on Monte Carlo procedures as follows. We generated 500 time series of soil moisture by resampling the original monthly series for each month using the same sequence for all the grid cells. This ensured that the time series of each sample retained the spatial correlation structure and seasonal variations of the original datasets. The area of significant local trends was then calculated for each resampled series and the 95th percentile calculated from the total sample. If the area of significant trends in the original data is greater than this percentile value then it is field significant. Using this method with a 5% local significance level, Andreadis and Lettenmaier (2006) calculated

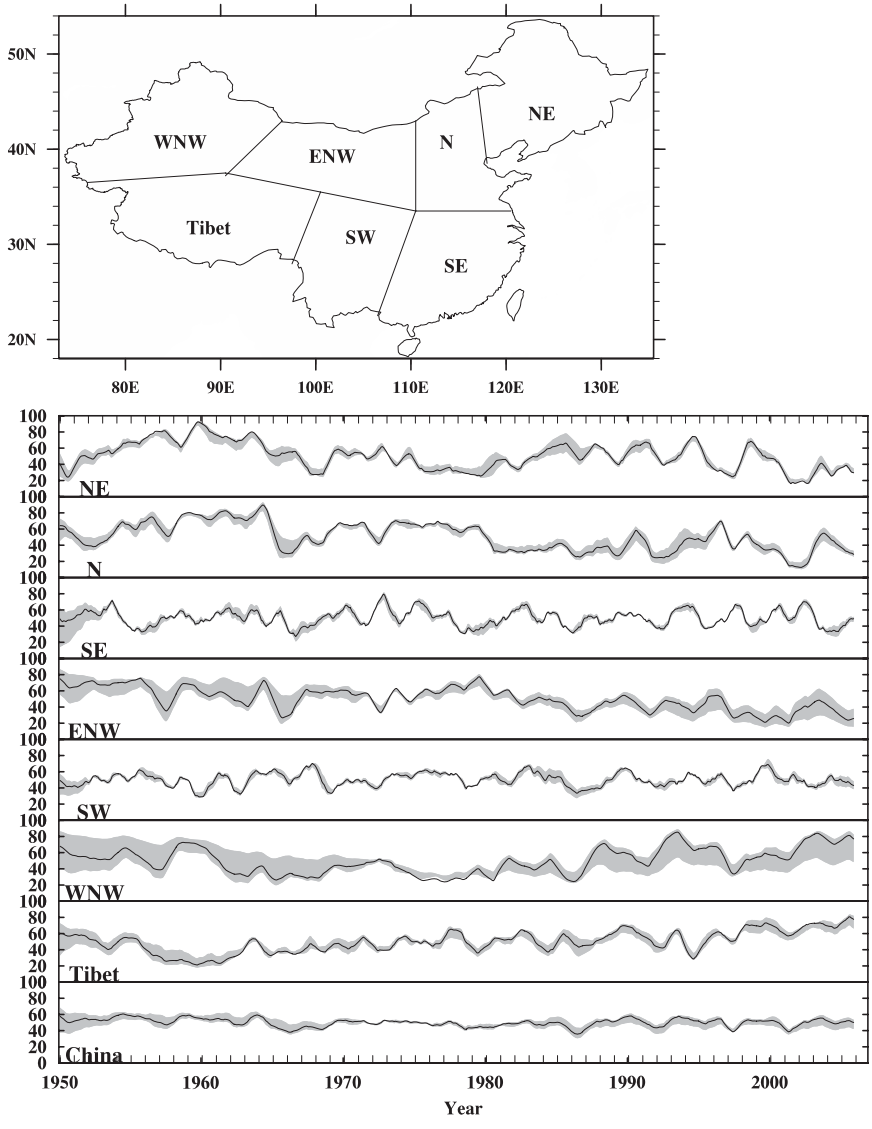

FIG. 1. (top) Location of regions (''China'' refers to the entire domain); (bottom) 13-month moving averages of soil moisture percentiles from the ensemble median (dark lines) and range of individual models (gray shading) for the seven regions and China.

that for a field significance level of 5%, the fraction of rejections needed to exceed 20.4% for soil moisture and 14.1% for runoff over the continental United States for the analysis period 1920–2003. We followed the same approach in our analysis of reconstructed soil moisture over China.

4. Results

a. Consistency of simulated soil moisture

To compare the regional disparities among different models, we divided the domain into seven subregions as indicated in the top panel in Fig. 1. The subregions are referred to as NE, N, SE, ENW, SW, WNW, and Tibet. (Note: Taiwan and Hainan both belong to SE, but we did not perform simulations over those areas because of inadequacies of forcing data for these relatively small islands.) The bottom panel in Fig. 1 shows 13-month moving averaged soil moisture percentiles for the ensemble percentiles over the seven subregions and over the entire domain. The shading indicates the envelope of percentiles from the four individual models. With the exception of WNW and part of the ENW region, the envelopes do not exhibit large discrepancies in most regions, implying that the models generally are consistent with each other. For some regions (e.g., SE and WNW) there seems to be large disparity between models at the start of the time period, indicating that

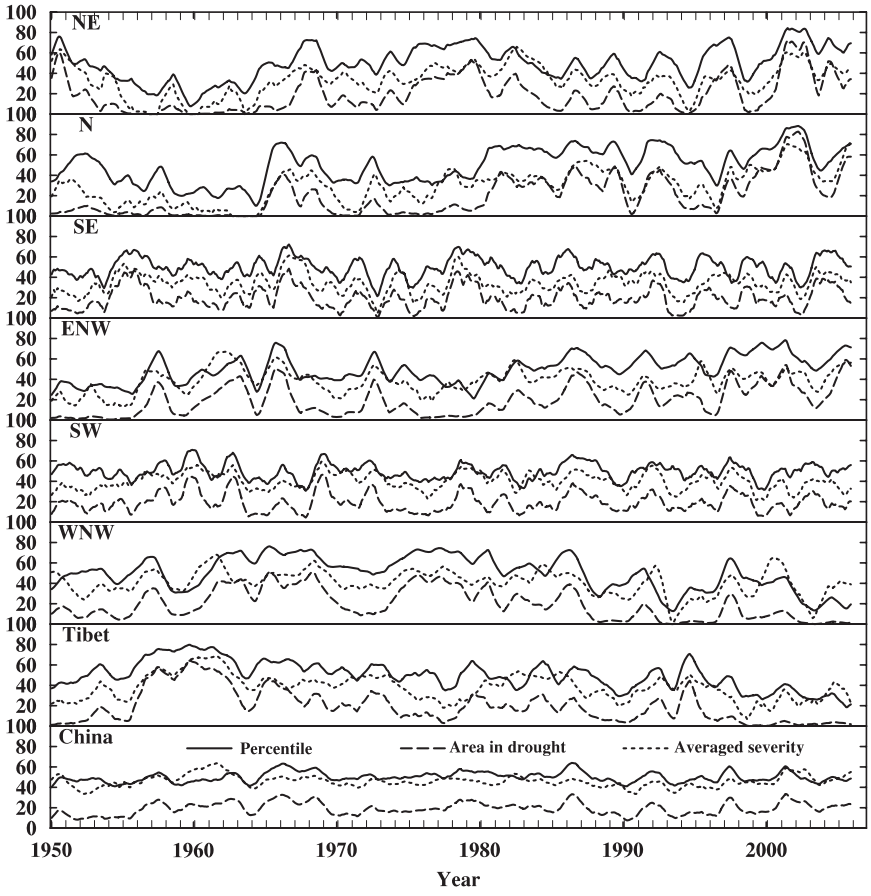

FIG. 2. The 13-month moving averages of soil moisture percentiles, percentage of region in drought, and average severity of area in drought averaged over each region and China. The percentage area in drought is the ratio of areas with soil moisture percentiles below 20% to total land areas within the China domain (except the regions without data). The average severity is the average soil moisture deficit with respect to the 20% in each month.

there may be some lingering initialization effects. Figure 1 does not show frequent drought occurrence (i.e., percentiles below the 20th) because of the smoothing inherent in the temporal moving average and the large areas over which the spatial averages were computed. Furthermore, while an entire region may not be in drought at a particular time, this does not preclude some part of the region being in drought.

Figure 2 shows the time series of averaged percentiles, averaged severity, and the percentage area in drought averaged over the subregions and the entire domain. For the entire domain, the averaged percentiles are about 50%, and the percentage of area in drought is typically about 25%, which is consistent with the PDSI data of Zou et al. (2005). The values of the average severities are comparable to the values of the averaged percentiles. Among all subregions, the temporal variation of the three drought indicators over SE and SW shows greater high-frequency variability than for the other regions. The high frequency of soil moisture variations over south China might relate to the variations of the East Asian monsoon precipitation (Zuo and Zhang 2007). With respect to timing of droughts, the lowest averaged percentiles are in the late 1960s in the N region, and after 2000 in the WNW region. On the other hand, the maximum severity appears in the early 2000s in the N region and the late 1980s for WNW.

Based on the time series shown in Fig. 2, Table 1 summarizes the top five months ranked by the averaged severity, area extent, and a combined metric of severity and area. The combined metric was computed as the averaged severity over the drought area multiplied by the total area in drought for each month. The most severe drought occurred in June 2003 over the northeast with a severity value of about 68%. For all five selected months, the average severity was larger than 63%. For the months ranked by spatial extent (second column in Table 1), the top five months all occurred in the second

TABLE 1. Five months with the largest average drought severity, spatial extent, and combined extent-of-severity metric. The date format is mm/yyyy.

Average severity (%)	Spatial extent (%)	Extent-of-severity metric
06/2003 (67.8)	10/1997 (40.4)	07/2001
12/1961 (67.4)	09/2001 (39.2)	10/2001
01/1962 (67.2)	07/2001 (38.9)	09/2001
11/1961 (67.0)	10/2001 (38.8)	10/1997
02/1962 (65.7)	11/1997 (38.7)	11/1997

half of 1997 and 2001, and the largest spatial extent covered 40.4% of the domain. If we consider the effect of both severity and area extent, July 2001 is the most prominent month, and the top five ranked months are the same as those for maximum spatial extent ranked in different order. Furthermore, all selected months in Table 1 actually belong to the same drought event (i.e., drought of 1997–2003) from the cluster analysis described in section 3b. The characteristics of this drought event will be further discussed in the following sections.

b. Cluster analysis and drought statistics

The ensemble soil moisture percentiles were used to identify drought extent using the cluster algorithm described in section 3. A total of 76 droughts with area greater than the 150 000 km^2 threshold were identified with durations longer than 3 months. Of those, the durations of 50 droughts were shorter than 6 months, and only 9 droughts lasted longer than 24 months. Table 2 lists the top five drought events ranked by the duration, maximum spatial extent, and averaged severity. The month with maximum spatial extent and averaged severity for each event is also given. Note that Table 2 refers to the characteristics of individual drought events (that last for 3 months or longer) and Table 1 refers to the characteristics of individual months. As described in section 4a, the selected months in Table 1 are based on the values of averaged severity and drought pixel areas in each individual month, and the adjacent months in the same drought event might be selected because they have very similar spatial extents. For Table 2, the spatial extent refers to the largest area for a specific drought event, and the selections are based on the cluster analysis described in section 3b. In terms of duration, the five longest droughts in descending order were 1997–2003 (76 months), 1964–70 (70 months), 1974–79 (64 months), 2004–06 (34 months), and 1962–64 (26 months). The 5 most spatially extensive droughts in descending order were 1997–2003 (40.4% of total area), 1986 (37.7%), 1987 (37.5%), 1979–81 (36.2%), and 1964–70 (35.8%).

TABLE 2. Five most prominent drought events in terms of duration, spatial extent, and average severity. In the second column, the monthly maximum fractional area in drought and the corresponding date are given in parentheses. In the third column, the monthly maximum severity and corresponding date are given in parentheses. The selected events in the second and third columns are based on the maximum values of the spatial extent and severity in each drought event. The date format is mm/yyyy.

Duration (months)	Spatial extent	Severity
1997–2003 (76)	1997–2003 (40.4%, 10/1997)	1997–2003 (67.8%, 06/2003)
1964–70 (70)	1986 (37.7%, 09/1986)	1961–64 (67.4%, 12/1961)
1974–79 (64)	1987 (37.5%, 03/1987)	1959–61 (63.3%, 05/1960)
2004–06 (34)	1979–81 (36.2%, 11/1979)	2004–06 (60.3%, 12/2006)
1962–64 (26)	1964–70 (35.8%, 08/1964)	1950–51 (59.6%, 10/1950)

Table 2 also shows that the 5 most severe drought events were 1997–2003 (67.8% maximum severity), 1961–64 (67.4%), 1959–61 (63.3%), 2004–06 (60.3%), and 1950–51 (59.6%). The drought of 1997–2003 stands out for being the second longest event (76 months), covering the largest area (40%), and having the highest severity (68%).

The plots in Fig. 3 show the peak spatial extent and severity distribution for the five major drought events. The selected months were chosen using a combined metric of severity and duration, calculated for each month as the average severity across the drought multiplied by drought area (Sheffield et al. 2009). The difference between this metric and the metric used in Table 1 is that it is calculated over the entire drought event rather than for an individual month. The peak month was identified for each event, and then the top five months in different drought events (among the 76 droughts) were chosen. From Fig. 3, we can see that each event broke into several centers. For example, the 1997–2003 drought mainly existed in the region between the Yellow and Yangtze Rivers and in northwestern Gansu province. The northeast was also affected by this drought, but the severity was smaller than for the other two regions. The 1964–70 drought was mostly in southeastern China, with a large drought center in September 1966 located over middle–lower areas of the Yangtze river basin, with several smaller drought centers located over Gansu and Xinjiang Provinces. The 1979–81 drought remained over southeast China while a smaller drought appeared over northeastern China. The 2004–06 drought was clearly divided into two centers, one located over inner Mongolia and another over Sichuan Province. On the basis of drought extent and average severity, the 1997–2003

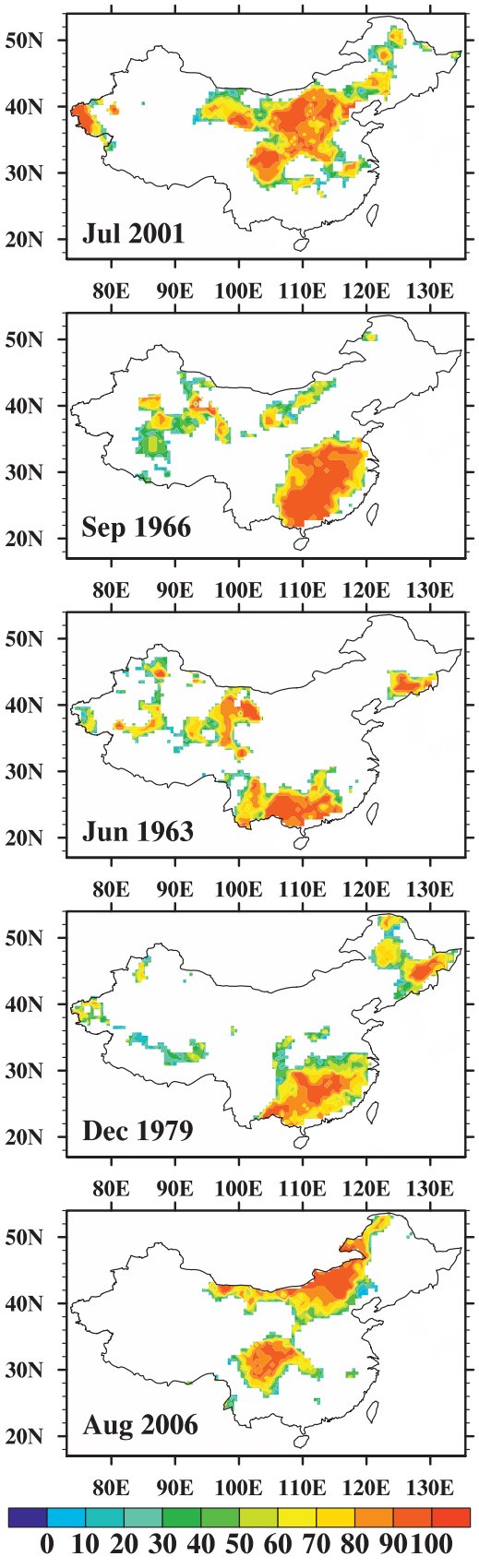

TABLE 3. Total number of drought events and the distribution of their duration as a function of the minimum area threshold used in the cluster algorithm.

Area threshold	No. of droughts	Duration ≤ 6 months	Duration ≥ 12 months	Duration ≥ 24 months
25 000 km^2	140	98	24	7
50 000 km^2	126	95	18	9
100 000 km^2	88	57	19	11
150 000 km^2	76	50	18	9
200 000 km^2	78	48	17	8

drought is the most prominent of record. The maximum extent was almost 3.9 million km^2 in July 2001, with an average severity of 68%. The drought covered all of the north and much of the central part of the country. In this respect our results are similar to station analyses using the PDSI (Zou et al. 2005) and a *Z* index (Wang et al. 2003).

c. *Variation of drought occurrences by areal threshold*

For the cluster analysis, the number of droughts identified depends on the areal threshold. Table 3 summarizes the total number of droughts for different durations and area thresholds. When the areal threshold is reduced from 200 000 to 25 000 km^2, the total number of droughts increases from 78 to 140. The largest differences in number of droughts is for the shortest drought life spans (i.e., <6 months), which increase from 48 to 98. For the longer durations (>12 months), the number of droughts changes less.

To examine the temporal variations of drought occurrences for the different area thresholds, we also counted the drought numbers for each month from the cluster analysis results. It should be noted that an individual drought might be counted repeatedly in different months depending on the duration. Figure 4 shows the monthly time series of the number of droughts for different areal thresholds. The figure shows that there are large variations of drought occurrence with the time of evaluation. The average number of droughts occurring

←

FIG. 3. Spatial distribution of severity of major droughts at their peak extent and severity. The calculation of severity is described in section 3b. The events were chosen by calculating a simple metric of the mean severity of all grid cells in a drought multiplied by the drought area for each month. The top five peak months were then selected. For example, July 2001 has the largest metric among the all events.

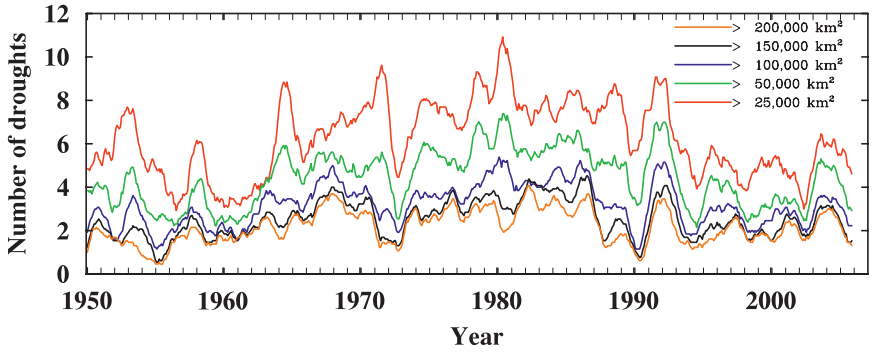

FIG. 4. The 13-month moving average of the number of droughts for different minimum area thresholds. An individual drought is defined as contiguous 0.5 cells with soil moisture percentiles below the 20th percentiles that last for at least one month.

in any month for areal thresholds ranging from the largest (>200 000 km^2) to the smallest (25 000 km^2) were 2.2, 2.5, 3.1, 4.4, and 6.2, with standard deviations of 1.1, 1.2, 1.4, 1.8, and 2.4, respectively. Droughts were relatively more frequent in the mid-1960s to early 1990s than in other periods, which are consistent with the results derived from PDSI and standardized precipitation index (SPI) analyses (Zhai et al. 2010).

d. *Severity–area–duration analysis*

To examine the relationship of drought severity and drought extent for individual events, we also plotted SAD curves for each duration. Figure 5 shows the results for durations of 3, 6, 12, 24, and 48 months for the selected major drought events. The selections are the same as in Fig. 3. For the 3-month duration, the 2004–06,

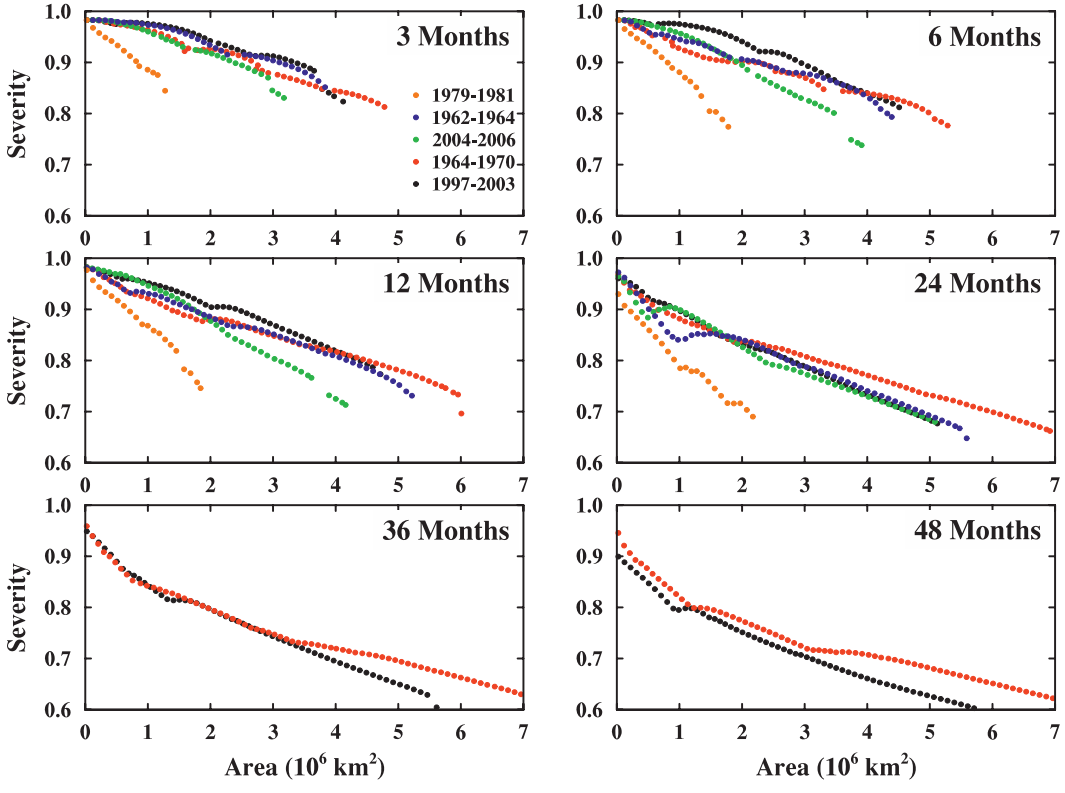

FIG. 5. SAD curves for durations of 3, 6, 12, 24, 36, and 48 months. Curves are shown for five major drought events. The drought selections are the same as in Fig. 3. The events shown in the legend are ordered downward by decreasing values of the metric. The calculation of severity is described in section 3b.

1997–2003, 1964–70, and 1962–64 droughts had similar severities for areas less than 1 million km^2; however, for the 24-month duration, only the 1964–70 drought had considerably lower severity than the other three. Among those five droughts, only the 1964–70 and 1997–2003 droughts last longer than 36 months. The duration of the 2004–06 drought was truncated by the end of the dataset; hence statistics for its 4-yr duration are not available. The 1979–81 drought was the least severe with relatively small areal extent compared with the others for all durations, but the slope of the curve at this areal extent is relatively sharper than for the other events. The 1964–70 drought had the largest spatial extent of the five events (up to about 7 million km^2), even though it did not have the highest severity in terms of averaged severity at the relative small area extents. Note that the drought of 1964–70 had the largest spatial extent compared to the other events only when its severity was relatively low. For higher severity values, the 1997–2003 drought is more spatially extensive, which is the reason that this drought is ranked highest in Table 2 in terms of spatial extent.

SAD envelope curves are constructed by choosing the maximum severity from all drought events at each duration and area increments. For purposes of our analysis, the area increment was taken as 20 grid cells (approximately 50 000 km^2). Figure 6 shows the envelope curves for predefined durations with respect to the drought spatial extents. Each point on the curve was derived from a specific drought event associated with a specific duration. The figure indicates that the 1997–2003 drought was pervasive in terms of both severity and spatial extent for areas smaller than 4 million km^2, whereas the 1964–70 drought was dominant for areas larger than 4 million km^2. Other drought events appear in the envelope curves only for relatively small areas for 12- and 6-month durations. The 2004–06 drought dominates for areas between 1 and 1.5 million km^2 for 12-month duration whereas the 1962–64 drought is the most severe event only for smaller areas. The 1950–51 drought does not appear on the SAD envelope plot because its spatial extent was relatively small.

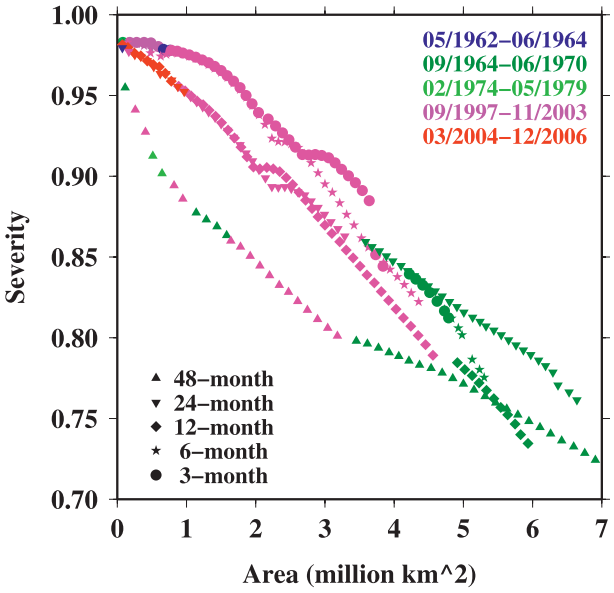

FIG. 6. SAD envelope curves for durations of 3, 6, 12, 24, 48 months. The envelopes were derived from the multimodel soil moisture percentiles. Colors indicate specific drought events.

e. *Trend analysis*

Figure 7 shows results of the application of the seasonal Mann–Kendall test to monthly time series of soil moisture, drought severity, drought duration, and drought frequency, all computed from the multimodel median. We followed Andreadis and Lettenmaier (2006) in constructing time series of drought duration for each grid cell by counting the number of consecutive months in drought (soil moisture percentile below 20%) during the total 684 months in the period 1950–2006. Drought severity for each grid cell was calculated as the cumulative departure of soil moisture from the drought threshold (20th percentage), averaged over the duration of each drought event. Drought frequency was defined as the inverse of the drought interval—the number of months between droughts. Then for each grid cell, the time series of drought frequency, duration, and severity were constructed. It should be noted that the length of these time series varies from grid cell to grid cell.

Figure 7a shows that locally significant (5% significance level) downward (drying) trends appear over northeastern China from Hilongjiang to the border of Xinjiang and Gansu provinces (1418 grid cells or about 37% of the land area), whereas upward (wetting) trends occur over most of Xinjiang, Qinhai, part of Tibet, and small areas over south China (1010 grid cells or 26% of the land areas). Zhai et al. (2005) analyzed trends in total precipitation and the frequency of daily precipitation extremes over China and found that annual total precipitation has significantly decreased over northeast China, north China, and over the Sichuan Basin but increased in western China, the Yangtze River valley, and the southeastern coast. The trend maps derived from soil moisture are generally consistent with these precipitation trends, with the exception of the Yangtze River valley, where soil moisture does not show significant upward trends. Because soil moisture trends are related to precipitation as well as to evaporative demand, which in turn is affected by surface air temperature, downward solar radiation, and other variables, soil moisture trends need

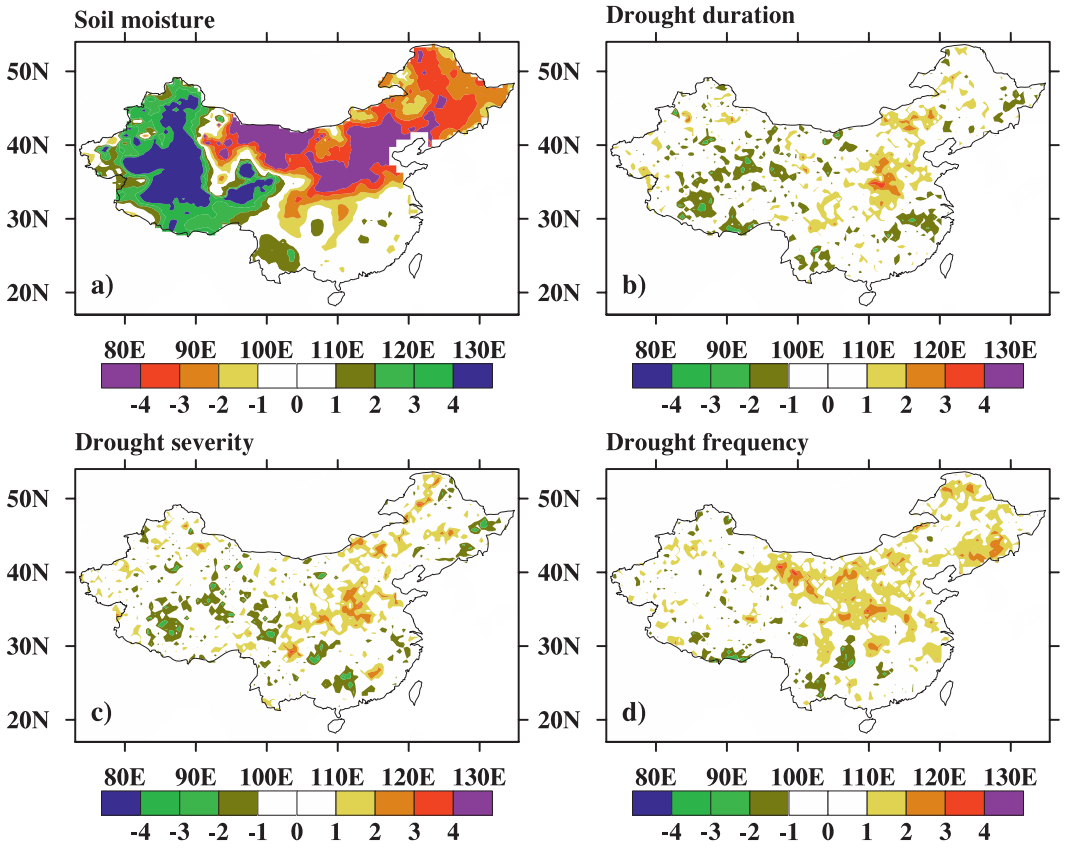

FIG. 7. Annual trends in (a) soil moisture percentile, (b) drought severity, (c) drought severity, and (d) drought frequency for 1950–2006. The trends were computed using the seasonal Mann–Kendall algorithm. The construction of time series of drought duration, severity, and frequency are described in section 4e. The different colors represent the magnitudes of the statistics.

not be consistent with trends in precipitation. Over the entire domain, the soil moisture trend results indicate that soil moisture decreased over much of China during the 1950 to 2006 period (i.e., 26% uptrend cells versus 37% downtrend cells over the whole domain).

Figure 7a shows that apparent trends in soil moisture are spatially clustered. This result, also found by Andreadis and Lettenmaier (2006) over the United States, is probably attributable in part to spatial correlation in the model forcing data (especially precipitation, but also, as noted above, in the variables that control evaporative demand). To address this issue, we used the method of Livezey and Chen (1983) as described in section 3c to test field significance of soil moisture percentiles and examine the effect of spatial correlation of soil moisture on the trend analysis. Figure 8 shows the histogram of the percentage of land area with locally significant trends as determined from the 500 resampled time series. The area fraction threshold of the 95th percentile (or 25 trials in a total of 500 trials) is 20.3%, indicating that the 59% (i.e., 22% of cells with uptrend plus 37% of cells with downtrend) combined total cells with significant trends are field significant. This threshold value is close to the value calculated by Andreadis and Lettenmaier (2006) over the conterminous United States. For drought variables (i.e., severity, duration, and frequency), it is not possible to perform a test of field significance because the time series for different grid cells have different lengths.

Figure 7b shows that upward trends in drought duration occurred from eastern inner Mongolia to eastern-central China (including Shanxi and Henan provinces), the western part of Xijiang, and a few cells over Sichuan province. The area of upward trends, however, was quite small (2.7% or 105 grid cells). The number of downward trends was only slightly smaller than the number of upward trends (2.3% or 91 cells) with locations of the downward trends very scattered, including the Tibetan Plateau and some cells over eastern China. The combined total of upward trends and downward trends in drought duration is too small to pass a test of field significance. Drought severity (Fig. 7c) increased in 159 cells (or 2% of the domain), with fewer downward trends (112 cells or 2.9%). Drought frequency (Fig. 7d) increased in 200 grid cells and decreased in 38 cells. A recent study of trends in PDSI and SPI indicated that

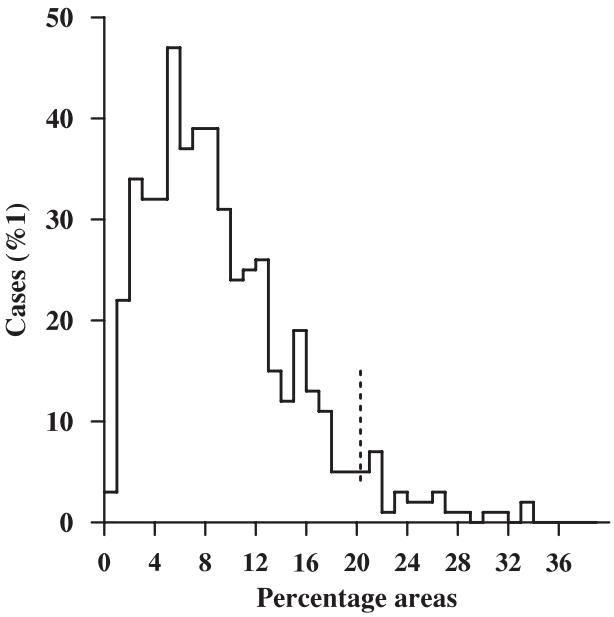

FIG. 8. Histogram of the percentage area of land for which a set of 500 time series of randomly sampled spatial fields of soil moisture with significant local trends. The 95th percentile (i.e., 25 cases of total 500 trials) is indicated by the dotted line and has a value of 20.3%, meaning that the occurrence of the trends in original data (i.e., 59% land areas) is significant, and the trends are not due to data spatial correlation.

frequency of drying years has increased over northeastern China and decreased over the northwest part of the country (Zhai et al. 2010). Our soil moisture work, while not indicating statistically significant trends, has the same general patterns.

5. Summary and conclusions

A common set of observation-based meteorology data was used to force four land surface models over China for the period 1950–2006. The soil moisture data from the individual models were combined into a multimodel estimate of soil moisture percentiles that reduces the uncertainty derived from the different model parameterizations of water and energy dynamics. The ensemble soil moisture percentiles data were then used to quantify the occurrence, space–time characteristics, and trends in soil moisture drought through SAD and cluster analysis methods. Our major conclusions are as follows:

1) A regional comparison between percentile time series derived from the individual models and the ensemble show that the models are generally consistent with each other over most regions, with the exception of western China, including WNW, ENW, and Tibet. The inconsistency in western China is likely due to the arid and semiarid climate and the complex topography of these regions, which emphasizes the differences in the model soil hydrology schemes.
2) For an area threshold larger than 150 000 km^2, 76 major droughts with life span 3 months or longer occurred in China during 1950–2006, and 50 of these droughts were shorter than 6 months. The longest drought event lasted 76 months from 1997 to 2003 over southwestern China. This drought is also the most spatially extensive one in the period of record and covered over 40% of China's land area in October 1997.
3) The 1997–2003 drought was the most prominent event in the period of record, with a spatial extent that peaked in October 1997 with an area of about 40% of the land area of China (or 3.9 million km^2). This drought dominated most of the SAD envelope curve for areas smaller than 5 million km^2. This drought was also identified in the global drought SAD analysis of Sheffield et al. (2009) as being particularly spatially extensive but was found to be of much shorter duration in that work, likely because of the higher minimum area threshold used. The droughts of 2004–06, 1997–2003, and 1964–70 had similar severities for areas less than 1 million km^2 at the 3-month durations. For the 12-month duration, the 1964–70 event dominated the SAD envelope curves for areas up to 5 million km^2. The drought of 1997–2003 contributed to most of the SAD envelope curve at all durations for area between 1 and 4 million km^2.The 2004–06 drought occupied the SAD envelope curve for small areas at the 12-month duration, but this drought was still developing in 2006, and thus its characteristics are uncertain.
4) An analysis of soil moisture trends shows spatially contiguous areas of drying over the northeast to north central China and wetting over most of the west including Xinjiang, Tibetan Plateau, and small areas over Yunnan province. The area with drying trends was much larger than the area with wetting trends (37% versus 22%) and passed a field significant test (with the threshold of 20.3% at the 0.05 significant level). Overall, there has been a general drying trend over China for the 1950–2006 study period with a concurrent increasing risk of drought (duration, severity, and frequency).

We used a multimodel ensemble approach to help reduce the uncertainty due to the bias of single model for investigating the characteristics and changes in drought. Multimodel ensemble analysis is a well-established technique in both climate prediction (e.g., Krishnamurti et al.

2000) and surface hydrological studies (e.g., Gao and Dirmeyer 2006). The combination of analysis methods we used (severity–area–duration, cluster, and trend analysis) is essential for determining drought characteristics and recognizes that drought is a multivariate process that is not physically restricted in time or in space by geographic or political boundaries. The trend analysis shows an overall increasing risk of drought over China during 1950–2006, which hints at a possible role of climate change. Precipitation and drought in China are dominated by the strength of the East Asian monsoon, which has weakened in terms of land–ocean pressure gradients over the past 30 years (Yu et al. 2004), shifting precipitation rain belts southward. The reasons for this are the subject of current research but are likely related to changes in land–ocean thermal contrasts and connections to ENSO activity (Lau et al. 2000; Dai et al. 2004) and northern Eurasian snow cover (Wu et al. 2009). Whether these changes have been forced by global warming or are part of the longer-term decadal variability seen over the past 100–150 years is unclear. Nevertheless, climate models project that a warmer and moister atmosphere in the future will actually lead to an enhancement of the circulation strength and precipitation of the summer monsoon over most of China (e.g., Sun and Ding 2010) that will offset enhanced drying due to increased atmospheric evaporative demand in a warmer world (Sheffield and Wood 2008).

Acknowledgments. This work was funded in part by the National Science Foundation of China under Grants 40905061 and 40830103, by the Department of Science and Technology of China under Grants 2009CB421403 and 2010CB428403, and by the U.S. National Oceanic and Atmospheric Administration (NOAA) under Cooperative Agreement NA08OAR4320899 to the University of Washington. We appreciate the assistance of Dr. Youlong Xia at NOAA's National Center for Environmental Prediction, who provided the NOAH model parameters. Three anonymous reviewers are thanked for their constructive comments, which substantially improved the manuscript.

REFERENCES

Andreadis, K. M., and D. P. Lettenmaier, 2006: Trends in 20th century drought over the continental United States. *Geophys. Res. Lett.,* **33,** L10403, doi:10.1029/2006GL025711.

——, E. A. Clark, A. W. Wood, A. F. Hamlet, and D. P. Lettenmaier, 2005: Twentieth-century drought in the conterminous United States. *J. Hydrometeor.,* **6,** 985–1001.

Bonan, G. B., S. Levis, L. Kergoat, and K. W. Oleson, 2002: Landscapes as patches of plant functional types: An integrating concept for climate and ecosystem models. *Global Biogeochem. Cycles,* **16,** 1021, doi:10.1029/2000GB001360.

Chen, F., Z. Janjic, and K. Mitchell, 1997: Impact of atmospheric surface-layer parameterizations in the new land-surface scheme of the NCEP mesoscale Eta model. *Bound.-Layer Meteor.,* **85,** 391–421.

Cong, Z., D. Yang, B. Gao, H. Yang, and H. Hu, 2009: Hydrological trend analysis in the Yellow River basin using a distributed hydrological model. *Water Resour. Res.,* **45,** W00A13, doi:10.1029/2008WR006852.

Dai, A. G., K. E. Trenberth, and T. T. Qian, 2004: A global dataset of Palmer Drought Severity Index for 1870–2002: Relationship with soil moisture and effects of surface warming. *J. Hydrometeor.,* **5,** 1117–1130.

Dickinson, R. E., K. W. Oleson, G. Bonan, F. Hoffman, P. Thornton, M. Vertenstein, Z.-L. Yang, and X. Zeng, 2006: The Community Land Model and its climate statistics as a component of the Community Climate System Model. *J. Climate,* **19,** 2302–2324.

Ek, M. B., K. E. Mitchell, Y. Lin, E. Rogers, P. Grunmann, V. Koren, G. Gayno, and J. D. Tarpley, 2003: Implementation of Noah land surface model advances in the National Centers for Environmental Prediction operational mesoscale Eta model. *J. Geophys. Res.,* **108,** 8851, doi:10.1029/2002JD003296.

Entin, J. K., A. Robock, K.Ya. Vinnikov, S. E. Hollinger, S. Liu, and A. Namkhai, 2000: Temporal and spatial scales of observed soil moisture variations in the extratropics. *J. Geophys. Res.,* **105** (D9), 11 865–11 877.

Gao, X., and P. A. Dirmeyer, 2006: Multimodel analysis, validation, and transferability study for global soil wetness products. *J. Hydrometeor.,* **7,** 1218–1236.

Grebner, D., and T. Roesch, 1997: Regional dependence and application of DAD relationships. *FRIEND '97—Regional Hydrology: Concepts and Models for Sustainable Water Resource Management,* IAHS Publ. 246, International Association of Hydrological Sciences, 223–230.

Guo, Z., and P. A. Dirmeyer, 2006: Evaluation of GSWP-2 soil moisture simulations, Part I: Inter-model comparison. *J. Geophys. Res.,* **111,** D22S02, doi:10.1029/2006JD007233.

Gupta, S. K., P. W. Stackhouse Jr., S. J. Cox, J. C. Mikovitz, and T. Zhang, 2006: Surface radiation budget project completes 22-year data set. *GEWEX News,* No. 6 (4), International GEWEX Project Office, Silver Spring, MD, 12–13.

Hamed, K. H., and A. R. Rao, 1998: A modified Mann–Kendall trend test for autocorrelated data. *J. Hydrol.,* **204,** 182–196.

Hansen, M. C., R. S. DeFries, J. R. G. Townshend, and R. Sohlberg, 2000: Global lands cover classification at 1-km spatial resolution using a classification tree approach. *Int. J. Remote Sens.,* **21,** 1331–1364.

Hirsch, R. M., J. R. Slack, and R. A. Smith, 1982: Techniques of trend analysis for monthly water quality data. *Water Resour. Res.,* **18,** 107–121.

Kalnay, E., and Coauthors, 1996: The NCEP/NCAR 40-Year Reanalysis Project. *Bull. Amer. Meteor. Soc.,* **77,** 437–471.

Koster, R. D., Z. Guo, R. Yang, P. A. Dirmeyer, K. Mitchell, and M. J. Puma, 2009: On the nature of soil moisture in land surface models. *J. Climate,* **22,** 4322–4335.

Krishnamurti, T. N., C. M. Kishtawal, Z. Zhang, T. E. LaRow, D. R. Bachiochi, C. E. Willifor, S. Gadgil, and S. Surendran, 2000: Multimodel ensemble forecasts for weather and seasonal climate. *J. Climate,* **13,** 4196–4216.

Lau, K.-M., K.-M. Kim, and S. Yang, 2000: Dynamical and boundary forcing characteristics of regional components of the Asian summer monsoon. *J. Climate,* **13,** 2461–2482.

Lawrence, P. J., and T. N. Chase, 2007: Representing a new MODIS consistent land surface in the Community Land Model (CLM 3.0). *J. Geophys. Res.,* **112,** G01023, doi:10.1029/2006JG000168.

Lettenmaier, D. P., E. F. Wood, and J. R. Wallis, 1994: Hydroclimatological trends in the continental United States, 1948–88. *J. Climate,* **7,** 586–607.

Liang, X., D. P. Lettenmaier, E. F. Wood, and S. J. Burges, 1994: A simple hydrologically based model of land surface water and energy fluxes for general circulation models. *J. Geophys. Res.,* **99,** 14 415–14 428.

Liu, C. M., and S. F. Zhang, 2002: Drying up of the Yellow River: Its impacts and counter-measures. *Mitigation Adapt. Strategies Global Change,* **7,** 203–214, doi:10.1023/A:1024408310869.

Livezey, R. E., and W. Y. Chen, 1983: Statistical field significance and its determination by Monte Carlo techniques. *Mon. Wea. Rev.,* **111,** 46–59.

Livneh, B., Y. Xia, K. E. Mitchell, M. B. Ek, and D. P. Lettenmaier, 2010: Noah LSM snow model diagnostics and enhancements. *J. Hydrometeor.,* **11,** 721–738.

Mann, H. B., 1945: Nonparametric tests against trend. *Econometrica,* **13,** 245–259.

Matthews, E., 1984: Vegetation, land use and seasonal albedo data sets: Documentation of archived data tape. NASA Tech. Memo. 86107, 12 pp.

——, 1985: Atlas of archived vegetation, land use, and seasonal albedo data sets. NASA Tech. Memo. 86199, 54 pp.

Maurer, E. P., A. W. Wood, J. C. Adam, D. P. Lettenmaier, and B. Nijssen, 2002: A long-term hydrologically based dataset of land surface fluxes and states for the conterminous United States. *J. Climate,* **15,** 3237–3251.

Mitchell, K. E., and Coauthors, cited 2001: The Community Noah Land Surface Model (LSM)—User's guide (v2.2). [Available online at http://www.emc.ncep.noaa.gov/mmb/gcp/noahlsm/Noah_LSM_USERGUIDE_2.7.1.htm.]

Mitchell, T. D., and P. D. Jones, 2005: An improved method of constructing a database of monthly climate observations and associated high-resolution grids. *Int. J. Climatol.,* **25,** 693–712.

Nijssen, B. D., G. M. O'Donnell, D. P. Lettenmaier, D. Lohmann, and E. F. Wood, 2001: Predicting the discharge of global rivers. *J. Climate,* **14,** 3307–3323.

Oleson, K. W., and Coauthors, 2007: CLM 3.5 documentation. 34 pp. [Available online at http://www.cgd.ucar.edu/tss/clm/distribution/clm3.5/CLM3_5_documentation.pdf.]

——, and Coauthors, 2008: Improvements to the Community Land Model and their impact on the hydrological cycle. *J. Geophys. Res.,* **113,** G01021, doi:10.1029/2007JG000563.

Qian, W., Q. Hu, Y. Zhu, and D.-K. Lee, 2003: Centennial-scale dry-wet variations in East Asia. *Climate Dyn.,* **21,** 77–89.

Robock, A., K. Y. Vinnikov, G. Srinivasan, J. K. Entin, S. E. Hollinger, N. A. Speranskaya, S. Liu, and A. Namkhai, 2000: The global soil moisture data bank. *Bull. Amer. Meteor. Soc.,* **81,** 1281–1299.

Schubert, S. D., M. J. Suarez, P. J. Pegion, R. D. Koster, and J. T. Bacmeister, 2008: Potential predictability of long-term drought and pluvial conditions in the U.S. Great Plains. *J. Climate,* **21,** 802–816.

Sheffield, J., and E. F. Wood, 2007: Characteristics of global and regional drought, 1950- 2000: Analysis of soil moisture data from off-line simulation of the terrestrial hydrologic cycle. *J. Geophys. Res.,* **112,** D17115, doi:10.1029/2006JD008288.

——, and ——, 2008: Projected changes in drought occurrence under future global warming from multi-model, multi-scenario, IPCC AR4 simulations. *Climate Dyn.,* **31,** 79–105, doi:10.1007/s00382-007-0340-z.

——, G. Goteti, F. Wen, and E. F. Wood, 2004: A simulated soil moisture based drought analysis for the United States. *J. Geophys. Res.,* **109,** D24108, doi:10.1029/2004JD005182.

——, ——, and E. F. Wood, 2006: Development of a 50-year high-resolution global dataset of meteorological forcings for land surface modeling. *J. Climate,* **19,** 3088–3111.

——, K. M. Andreadis, E. F. Wood, and D. P. Lettenmaier, 2009: Global and continental drought in the second half of the twentieth century: Severity–area–duration analysis and temporal variability of large-scale events. *J. Climate,* **22,** 1962–1981.

Song, L. C., and Coauthors, 2005: The historical change of drought. *Drought—The Hot Topic of Global Change* (in Chinese), D. H. Qin, Ed., Chinese Meteorology Press, 9–27.

Su, B., Z. W. Kundzewicz, and T. Jiang, 2008: Simulation of extreme precipitation over the Yangtze River Basin using Wakeby distribution. *Theor. Appl. Climatol.,* **96,** 209–219.

Sun, Y., and Y.-H. Ding, 2010: A projection of future changes in summer precipitation and monsoon in East Asia. *Sci. China Earth Sci.,* **53,** 284–300.

Svoboda, M., and Coauthors, 2002: The drought monitor. *Bull. Amer. Meteor. Soc.,* **83,** 1181–1190.

Wang, A., K. Y. Li, and D. P. Lettenmaier, 2008: Integration of the variable infiltration capacity model soil hydrology scheme into the community land model. *J. Geophys. Res.,* **113,** D09111, doi:10.1029/2007JD009246.

——, T. J. Bohn, S. P. Mahanama, R. D. Koster, and D. P. Lettenmaier, 2009: Multimodel ensemble reconstruction of drought over the continental United States. *J. Climate,* **22,** 2694–2712.

Wang, Z. W., P. Zhai, and H. Zhang, 2003: Variation of drought over northern China during 1950–2000. *J. Geogr. Sci.,* **13,** 480–487.

Woodhouse, C. A., and J. T. Overpeck, 1998: 2000 years of drought variability in the central United States. *Bull. Amer. Meteor. Soc.,* **79,** 2693–2714.

Wu, B. Y., K. Yang, and R. Zhang, 2009: Eurasian snow cover variability and its association with summer rainfall in China. *Adv. Atmos. Sci.,* **26,** 31–44.

Xin, X., R. Yu, T. Zhou, and B. Wang, 2006: Drought in late spring of South China in recent decades. *J. Climate,* **19,** 3197–3206.

Xu, J., 2004: A study of anthropogenic seasonal rivers in China. *Catena,* **55,** 17–22.

Yu, R., B. Wang, and T. Zhou, 2004: Tropospheric cooling and summer monsoon weakening trend over East Asia. *Geophys. Res. Lett.,* **31,** L22212, doi:10.1029/2004GL021270.

Zhai, J., B. Su, V. Krysanova, T. Vetter, C. Gao, and T. Jiang, 2010: Spatial variation and trends in PDSI and SPI indices and their relation to streamflow in 10 large regions of China. *J. Climate,* **23,** 649–663.

Zhai, P., X. Zhang, H. Wan, and X. Pan, 2005: Trends in total precipitation and frequency of daily precipitation extremes over China. *J. Climate,* **18,** 1096–1108.

Zou, X., P. Zhai, and Q. Zhang, 2005: Variations in droughts over China: 1951–2003. *Geophys. Res. Lett.,* **32,** L04707, doi:10.1029/2004GL021853.

Zuo, Z., and R. Zhang, 2007: The spring soil moisture and the summer rainfall in eastern China. *Chin. Sci. Bull.,* **52,** 3310–3312.